International Journal of Thermophysics, Vol. 27, No. 3, May 2006 (© 2006)
DOI: 10.1007/s10765-006-0065-y

A High-Temperature, Thermal Non-equilibrium Equation of State for Ammonia

D. L. Allison[1] and P. G. Mikellides[1,2]

Received September 12, 2005

The engineering applications of ammonia extend far beyond the pressure and temperature ranges for which thermodynamic models currently exist in the literature. Thus, a thermal non-equilibrium thermochemical model was developed to compute the composition and thermodynamic properties of ammonia for an extended temperature and pressure range that includes ionization reactions. Thermal non-equilibrium between electrons and heavy particles was included and is presented for ratios of $\frac{1}{2}$, 1, 2, and 3. The fourteen-equation nonlinear system produced under the assumptions of ideal gas and two-temperature local thermodynamic equilibrium was solved numerically using a Newton-Raphson method. The thermochemical model is verified for both the composition and thermodynamic properties by comparisons to existing thermochemical models in the literature. These comparisons verify the model for the available, yet limited, temperature and density ranges. Analysis of the composition and thermodynamic properties as a function of the independent properties confirms the necessity for such a model as part of rigorous computations with computational fluid dynamics (CFD) or magnetohydrodynamics (MHD) computer codes. The model can be easily cast in tabular form to complement the set of conservation equations utilized by such codes.

KEY WORDS: ammonia; electric rocket propellant; equation of state; high-temperature thermochemical model; thermal non-equilibrium

1. INTRODUCTION

The availability of two-temperature equations of state (EOS) for plasma temperature and low pressure ranges in polyatomic gases is

[1] Department of Mechanical and Aerospace Engineering, Arizona State University, P.O. Box 876101, Tempe, Arizona 85287-6106, U.S.A.
[2] To whom correspondence should be addressed. E-mail: Pavlos.Mikellides@asu.edu

0195-928X/06/0500-0794/0 © 2006 Springer Science+Business Media, Inc.

limited. For the case of ammonia, they are simply non-existent, as its applications have traditionally been at low/moderate temperature and moderate pressure ranges (e.g., refrigerants, etc.). However, this is no longer the case, as ammonia has been utilized for a more diverse range of applications. One particular area is related to deep space exploration missions that require rocket propulsion systems of high specific impulse. Electric propulsion rockets can provide such performance characteristics, which render them essential to many interplanetary missions. Chemical propulsion combustion reactions can be analyzed using an EOS within a range of low temperature and high pressure. Propellants utilized by electric propulsion rockets, on the other hand, operate in very high temperature and very low pressure regimes. Ammonia has indeed been used in electric propulsion applications such as the arcjet [1] and the pulsed inductive thruster and has shown great promise as the propellant of choice by producing uniquely elevated efficiency values [2]. Proper theoretical analysis and understanding of the behavior of ammonia within such devices and other possible applications demands the development of an appropriate equation of state model that can be employed in conjunction with proper numerical codes. In particular, such a thermochemical model – which is most likely to be used in tabular form – will complete the set of hydrodynamic or magnetohydrodynamic partial differential equations that describe the behavior of the gas/plasma within the application of interest.

The model is developed using fundamental statistical mechanics principles and appropriate assumptions. This approach initially allows calculation of ammonia's composition at several heavy-particle temperature (T_h), electron temperature (T_e), and density (ρ) values within the range of $1.0 \times 10^{-7}\,\mathrm{kg{\cdot}m^{-3}} < \rho < 1.0 \times 10^{-1}\,\mathrm{kg{\cdot}m^{-3}}$ and $0.00862\,\mathrm{eV} < T_e < 50\,\mathrm{eV}$ ($100\,\mathrm{K} < T_e < 580222\,\mathrm{K}$) and varying temperature ratio, $\theta = T_e/T_h$. The model then proceeds to calculate the thermodynamic properties as a function of ρ, T_e, and T_h which are verified using limited, but similar models from various literature sources.

2. APPROACH

2.1. Calculation of the Composition

The algorithm for determining the relative concentration of each species was subject to two main assumptions; the gas was assumed to behave as ideal and be in local thermodynamic equilibrium (LTE). The system of nonlinear algebraic equations that arises from the choice of chemical reactions was solved for concentrations of fourteen different species over the extended ρ, T_e, and T_h range of interest. Since, in general, the

range considered involves high temperature and low pressure values only, the dominant species expected in the mixture throughout those ranges are considered as part of the system. The fourteen species include the molecules NH_3, H_2, and N_2 and the atoms N and H. Ionization reactions were fully considered with the H^+ ion and all seven possible N ions along with the electron (e^-) species.

Other species could have been included, but their concentrations were confirmed as negligible. A past ammonia composition model computed for one-temperature and atmospheric pressure conditions by Beaumont showed that other species that could have been considered can, in fact, be ignored [3]. Although Beaumont's model only covers dissociation temperature ranges (950 to 2400 K), at higher temperatures where all molecules have basically dissociated, all possible monatomic ions for H and N have been included in the current model.

Therefore, the only relevant question as to which species can be safely neglected concerns those species which form at the lower dissociation temperatures. Figure 1 demonstrates that species like NH_2, NH, and N_2H_2 are about seven, eight, and eleven orders of magnitude less in concentration, effectively excluding each as important to the overall mixture properties. In addition, the presence of molecular ions, e.g., N_2^+ and H_2^+, is also excluded as it has been confirmed that they are negligible for moderate ion-to-electron temperature ratio (θ) values [4].

The choice of the most probable chemical reactions is subject to the requirements that they are linearly independent and that each species considered is included in at least one of the reactions. The following equations are the eleven reactions considered in this ammonia model and constitute the reaction path.

$$2NH_3 \leftrightarrow N_2 + 3H_2 \tag{1}$$

$$N_2 \leftrightarrow 2N \tag{2}$$

$$H_2 \leftrightarrow 2H \tag{3}$$

$$N^{Z+} \leftrightarrow N^{(Z+1)+} + e^- \qquad (\text{where } Z = 0 \text{ to } 6) \tag{4}$$

$$H \leftrightarrow H^+ + e^- \tag{5}$$

By employing the law of mass action,

$$K_p(T) = \prod_i P_i^{\nu_i} \tag{6}$$

where P_i's are the partial pressures and ν_i's are the stoichiometric coefficients of the reaction species (negative for reactants and positive for products), along with three conservation equations,

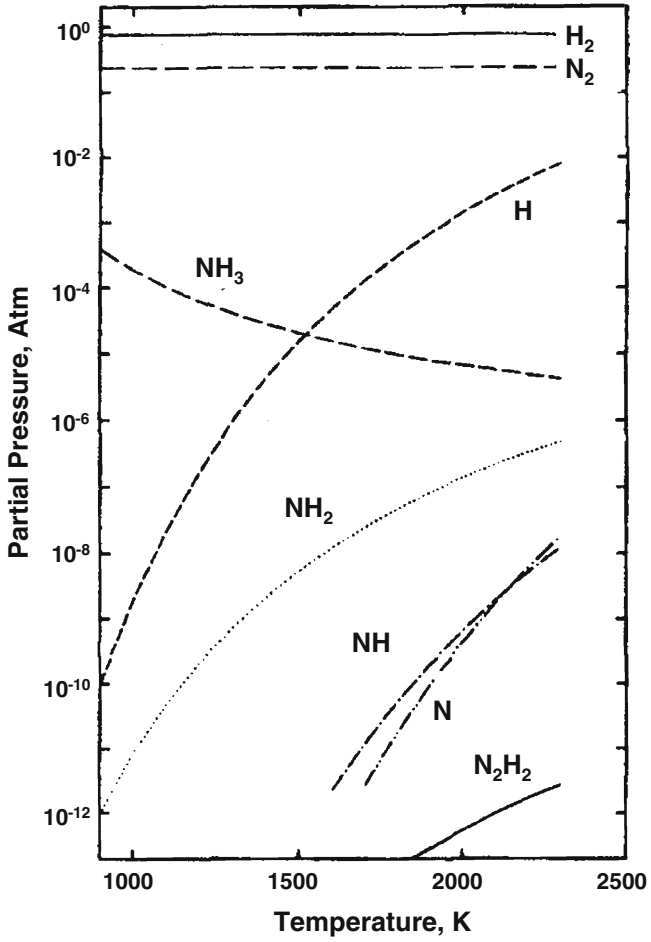

Fig. 1. Beaumont composition results for a one-temperature, ideal-gas model including dissociation reactions. The model confirms that certain species can be safely neglected. (1 bar = 10^5 Pa.)

$$\sum_i P_i = P \tag{7}$$

$$\frac{2P_{N_2} + P_N + \sum_{Z=1}^{7} P_{N^{Z+}}}{2P_{H_2} + P_H + P_{H^+}} = \frac{1}{3} \tag{8}$$

$$P_{e^-}\left(\frac{T_h}{T_{e^-}}\right) = \sum_{Z=1}^{7} Z P_{N^{Z+}} + P_{H^+} \tag{9}$$

the system comprises fourteen nonlinear coupled equations. Since there are eleven reactions that make up the system, Eq. (6) effectively represents eleven different equations. The three conservation equations that complete the system are Dalton's Law, the conservation of nuclei, and the conservation of charge (quasi-neutrality condition) shown above in Eqs (7), (8), and (9), respectively. The value of the equilibrium constant can be computed by

$$K_P(T_i) = \left(\frac{\mathrm{k}T_i}{V}\right)^{\sum \nu_i} e^{\frac{-\Delta\varepsilon_0}{\mathrm{k}T_i}} \prod Q_i^{\nu_i}, \tag{6a}$$

thus making the fourteen concentration values (represented as partial pressures, P_i, in the above equations) the only unknowns. Here k is the Boltzmann constant, V is the volume of the system (which is held constant), T_i is the temperature (T_e for ionization reactions and T_h for all other reactions), and $\Delta\varepsilon_0$ is the change in zero-point energy.

The total partition function, (Q_i) in Eq. (6a) is species dependent and includes the translational partition function for all particles, the vibrational and rotational partition functions for molecules, and the electronic contribution for all particles except for N^{+7}, H^+, and e^- [5,6]. The translational, rotational, vibrational, and electronic partition functions are given below. The rotational and vibrational partition functions for non-linear polyatomic and diatomic molecules are different and are distinguished below.

$$Q_\mathrm{trans} = \left(\frac{2\pi m\mathrm{k}T}{\mathrm{h}^2}\right)^{\frac{3}{2}} V \tag{10}$$

Here m is the mass of a species particle, h is Planck's constant, and T is the temperature of the species. If the species is an electron, the temperature is T_e while it would be T_h for all other species.

$$Q_\mathrm{rot}^\mathrm{nonlinear\_polyatomic} = \frac{\sqrt{\pi}}{\sigma}\left(\frac{8\pi^2\mathrm{k}T}{\mathrm{h}^2}\right)^{\frac{3}{2}} (I_\mathrm{A} I_\mathrm{B} I_\mathrm{C})^{\frac{1}{2}} \tag{11}$$

$$Q_\mathrm{rot}^\mathrm{diatomic} = \frac{8\pi^2 I\mathrm{k}T}{\sigma h^2} \tag{12}$$

Here σ is the symmetry number which is equal to 3 for ammonia and 2 for the diatomic molecules. The moment of inertia on each bonding axis

is represented by I_A, I_B, and I_C for the three bonds in NH_3 and I for the one bond in the diatomic molecules,

$$Q_{\text{vib}}^{\text{nonlinear\_polyatomic}} = \prod_{j=1}^{3N-6} \frac{1}{1 - e^{\frac{-\text{h}\omega_j}{\text{kT}}}} \tag{13}$$

$$Q_{\text{vib}}^{\text{diatomic}} = \frac{1}{1 - e^{\frac{-\text{h}\omega}{\text{k}T}}} \tag{14}$$

where N is the number of atoms that make up the molecule, and ω is the frequency of a vibrational mode.

The sum involved in the electronic partition function,

$$Q_{\text{el}} = \sum_{j=0}^{\infty} g_j e^{-\frac{\varepsilon_j}{\text{k}T}} \tag{15}$$

where ε is the energy of the energy level "j" and g is the degeneracy, is divergent. At high energy levels, the ground state and the excited state energy difference (ε_j) approaches the constant ionization potential and the term in the sum is then summed to infinity. In addition, the statistical weight, g_j, approaches infinity as the energy approaches the ionization potential [7]. These two problems are easily resolved as one considers that these particles are not isolated, but are part of a continuum and thus subject to interactions. The neighboring particles' higher energy levels interfere with the particles' own higher energy levels and thus effectively decrease the ionization potential. This lowered energy level where the ionization reaction occurs effectively reduces the number of allowable quantum levels from infinity to some finite limit. An expression used to establish the highest principle quantum number as the upper bound on the sum in Eq. (15) is

$$n^{\text{cutoff}} = \left(\frac{Z_{\text{eff}} (n_i)^{-1/3} \left(\frac{4\pi}{3}\right)^{1/3}}{a_0} \right)^{1/2} \tag{16}$$

where n^{cutoff} is the principle quantum number, α_0 is the Bohr radius, and n_i is the number density of that species [8].

2.2. Numerical Model

This system of the fourteen nonlinear coupled set of equations was solved using the Newton-Raphson method briefly stated as

$$J \cdot \delta x = -F. \tag{17}$$

Here, J is the Jacobian matrix and F is a vector of the fourteen equations that contains the species concentrations to be computed from Eqs (6)–(9). This results in a 14×14 Jacobian matrix and a 14×1 F vector, while δx is the corrections vector to the set of current concentrations in the iteration, the very first F-vector of an iteration being set to an initial estimate. The corrections vector is progressively added to the current set of concentrations and the updated set becomes the current initial estimate. The iteration proceeds until convergence is reached based on a chosen tolerance value.

The Jacobian can be analytically determined as the fourteen equations are easily differentiable. This implies that the derivatives computed to form the Jacobian do not need to be found numerically, which enhances the accuracy and stability of the code. The Jacobian for this system can easily be determined from the general expression,

$$J(n_1, \ldots, n_{14}) = \begin{bmatrix} \dfrac{\partial F_1}{\partial n_1} & \cdots & \dfrac{\partial F_1}{\partial n_{14}} \\ \vdots & \ddots & \vdots \\ \dfrac{\partial F_{14}}{\partial n_1} & \cdots & \dfrac{\partial F_{14}}{\partial n_{14}} \end{bmatrix} \tag{18}$$

where n_i represents the concentration of each species, i.

2.3. Calculation of the Thermodynamic Properties

Calculation of the gas mixture composition as a function of ρ, T_e, and T_h allows computation of the thermodynamic properties, since they are directly related to the total partition function. The total partition function is different for each species, as was previously explained. The particular expressions for each thermodynamic property are shown in Eqs (19)–(24) [9–11]. All quantities are calculated in their specific (per mass) form and are therefore denoted by their lower-case symbols. The entropy is represented by s, Gibbs free energy is g, internal energy is e, enthalpy is h, specific heat at constant pressure is C_p, and *nfe* is the number of free electrons, which signifies the average charge of the plasma mixture.

$$s = R_i \left(\ln \frac{Q^{\text{tot}}}{N} + 1 \right) + R_i T_i \left(\frac{\partial \ln Q^{\text{tot}}}{\partial T} \right) \tag{19}$$

$$g = -R_i T_i \ln \frac{Q^{\text{tot}}}{N} \tag{20}$$

$$e = R_i T_i^2 \left(\frac{\partial \ln Q^{\text{tot}}}{\partial T} \right)_{N,V} \tag{21}$$

$$h = e + Pv = R_i T_i^2 \left(\frac{\partial \ln Q^{\text{tot}}}{\partial T} \right)_{N,V} + R_i T_i \tag{22}$$

$$Cp = \left(\frac{\partial h}{\partial T} \right)_P \tag{23}$$

$$nfe = \frac{n_{\text{e}}}{n_{\text{ions}} + n_{\text{neutrals}}} \tag{24}$$

where R_i is the species' specific gas constant. The thermal non-equilibrium condition is invoked through the partition functions and the temperature variables that appear in the thermodynamic property expressions above. For each property that is calculated for the electron species, the temperature $T = T_{\text{e}}$, and for all other species $T = T_{\text{h}}$. This applies to both the partition function expressions and the property expressions. Of course, since the partition functions are changed by including thermal non-equilibrium, this also affects the composition calculation as well as the thermodynamic property calculations.

Using the composition data, the total mixture properties can be found using each species' respective mass fraction, c_{i}, which is ascertained from the composition solution. The specific internal enthalpy equation is used as an example [12].

$$h = \sum_{1}^{14} c_i h_i + \sum_{1}^{14} c_i (\Delta h_f)_i^0 \tag{25}$$

The internal energy and enthalpy both require that the zero-point energy be added to each species' contribution, as shown in the second term on the right-hand side of Eq. (25). This is because Eq. (22) (the statistical mechanical result) is really the total specific enthalpy above the zero-point reference. Therefore, to find the total enthalpy, the zero-point energy must be added. Since the absolute value of the zero-point energy cannot be calculated, the effective zero-point energy or chemical enthalpy is used. This is, for practical purposes, the specific heat of formation at absolute zero [13,14].

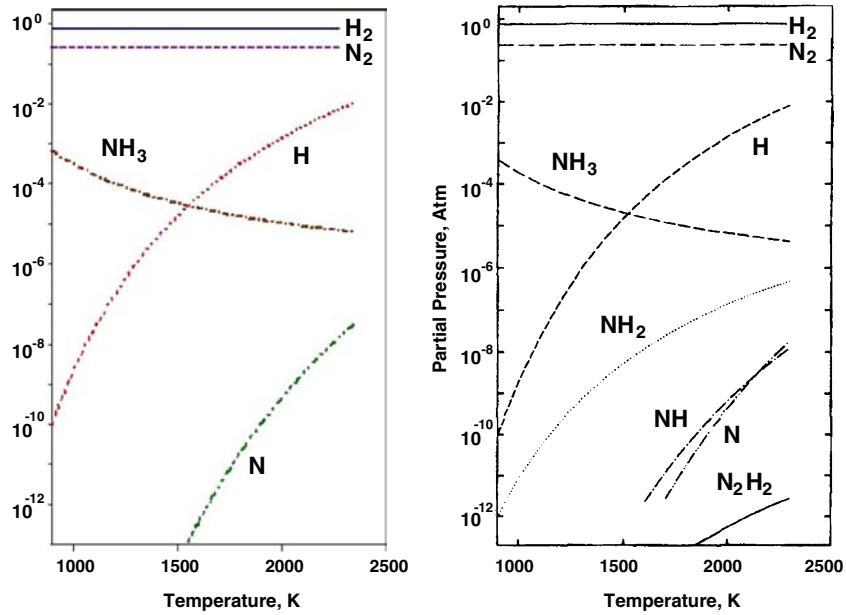

Fig. 2. Code composition output (left) compared with Beaumont composition output (right).

3. COMPOSITION VERIFICATION

3.1. Dissociation Temperature Range

The composition calculated by the current model is compared to models found in the literature. As there are no known ammonia thermochemical models that address the temperature and density ranges considered in this model, the available models are used to verify the code routines. Due to the limited models for comparisons, Beaumont's model [3] is used to verify the dissociation temperature range portion of the calculated equation of state. Figure 2 shows good agreement between the code output on the left and Beaumont's findings on the right.

Even though rigorous quantitative comparisons are difficult to perform, due to a lack of additional data from Beaumont besides the graph above, several quantitative observations can be made that lend credence to the model's validity for this temperature range. The mixture's composition is dominated by molecular nitrogen and hydrogen, both of which show very good agreement. At higher temperatures, atomic hydrogen is the next most significant presence and it is also in excellent agreement between the two models. The code's NH_3 variation predicts a slightly

higher composition than that of Beaumont, which can be attributed to the exclusion of the additional reactions that produce NH_2, NH, and N_2H_2. However, close inspection of the discrepancy reveals that the absolute error between the two NH_3 results can be estimated as 3×10^{-9} Pa at the low temperature and drops to 5×10^{-11} Pa at the highest temperature signifying a negligible discrepancy between the mixtures' thermodynamic properties.

3.2. Ionization Temperature Range

Due to the lack of relevant NH_3 models in the literature, the code was modified to perform calculations for the diatomic nitrogen and hydrogen cases and compared to results from Boulos et al. [15] in the ionization temperature regime. The modifications merely entailed changing the system to be solved. The reactions for the N_2 case started with the dissociation of N_2 and also include the ensuing nitrogen ionizations. The system for H_2 was similar to that of N_2, except that there was only one ionization reaction included.

Figure 3 shows the hydrogen composition comparison between Boulos et al. [15] and the code composition output depicted by the solid lines. The overall agreement between the two models is very encouraging with slight discrepancies of negligible significance. The discrepancy between the H_2 predictions occurs in a region where the concentration is at least three orders of magnitude less than the maximum and is a consequence of the exclusion of the negatively-charged hydrogen ion by the current effort. The H composition calculation also displays a slight disagreement; however, the error at 25000 K is approximately 0.25% between the H variation and the concentration of the dominant H^+ and e^- species, thus effectively eliminating its overall effect on the plasma mixture.

Figure 4 depicts comparisons between the Boulos et al. [15] model and the code output for nitrogen. The overall quantitative agreement between the two models is once again very good with slight discrepancies mostly attributed to the exclusion of certain species by the current effort. Furthermore, most of such discrepancies generally occur when the species is not a dominant part of the whole gas/plasma mixture thermodynamic state. Specifically, the discrepancy in the N^{++} predictions occurs when the species is two to three orders of magnitude less in concentration, and it converges to findings of Boulos et al. at 25000 K where it begins to reach the higher and more important concentrations. The divergence of the N^+ and e^- species and N species are coupled, as the N^+ species is higher in concentration than that of Boulos et al. while the N species is lower.

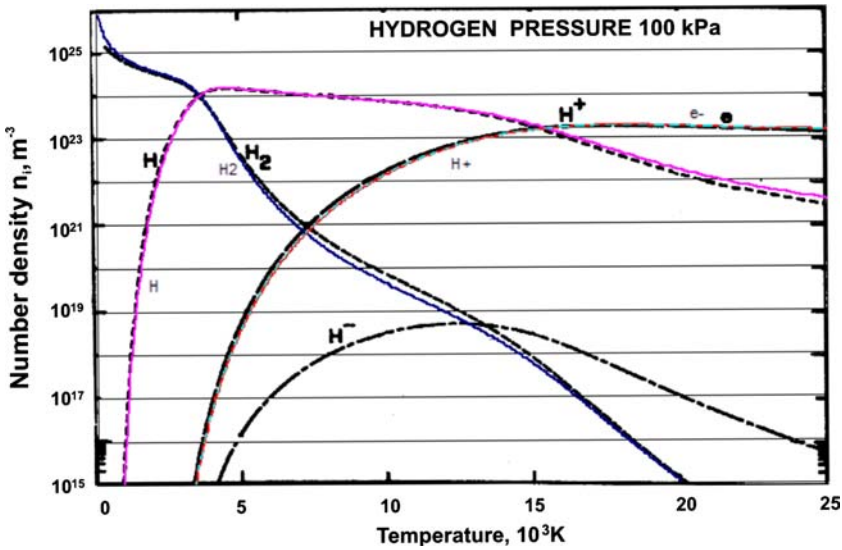

Fig. 3. Modified code composition output compared to Ref. 15 findings for diatomic hydrogen.

The N variance is approximately 1% when compared to the concentrations of N^+ and e^-.

The disagreement between the N^+ and e^- species' concentrations can be attributed to a different cut-off criterion, a different iteration tolerance, or even slightly different spectroscopic data. However, all aforementioned minor differences between the code and literature composition results do not collectively affect the accuracy of the computed thermodynamic properties as shown in the following section.

4. THERMODYNAMIC PROPERTY VERIFICATION

4.1. NIST-JANAF Comparison

The NIST-JANAF tables [16] are used to validate the thermodynamic properties calculated by the code using Eqs (19)–(23). Even though the JANAF tables do not include chemical reactions, useful comparisons can still be performed to verify the code's partition function and thermodynamic property calculations for the polyatomic molecule. The partition functions for ammonia are calculated and the mass fraction for NH_3 is merely set to unity, effectively constraining the mixture so that NH_3 is the only species allowed to exist. Figures 5–8 show the code and the JANAF

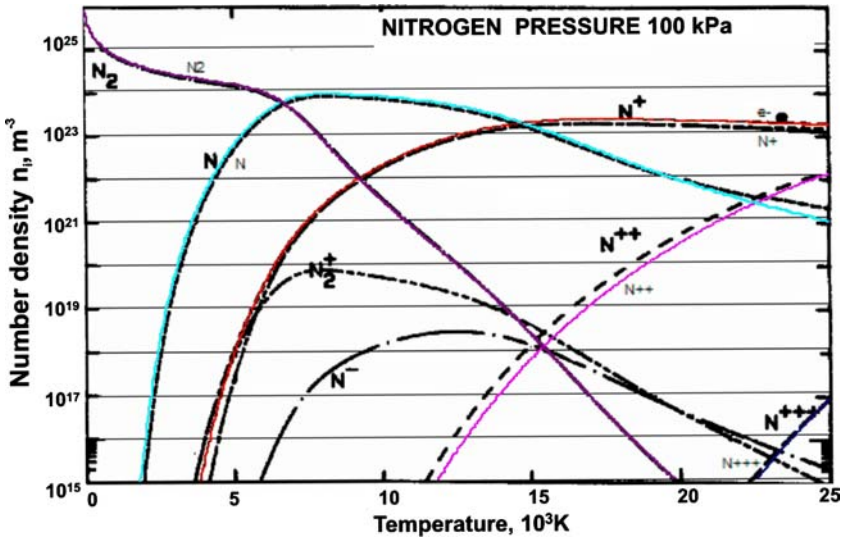

Fig. 4. Modified code composition output compared to Ref. 15 findings for diatomic nitrogen.

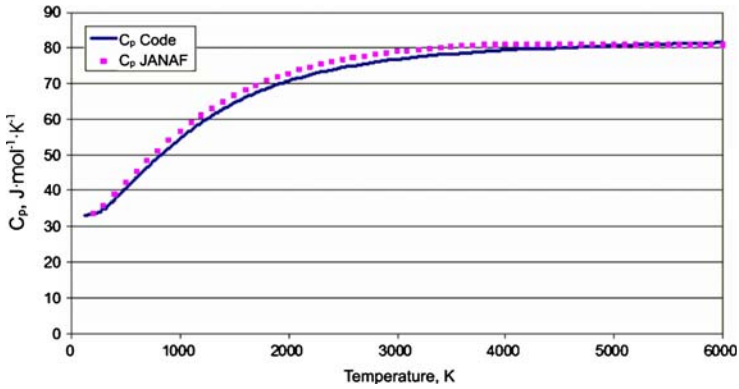

Fig. 5. Comparison of the specific heat at constant pressure, C_p.

NH_3 table thermodynamic property comparisons. The maximum temperature in Ref. 16 is 6000 K, and in this temperature range, each code-output thermodynamic property is in fairly good agreement with the JANAF model.

The above comparisons simply confirm the translational, rotational, and vibrational energy mode calculations for the polyatomic molecule.

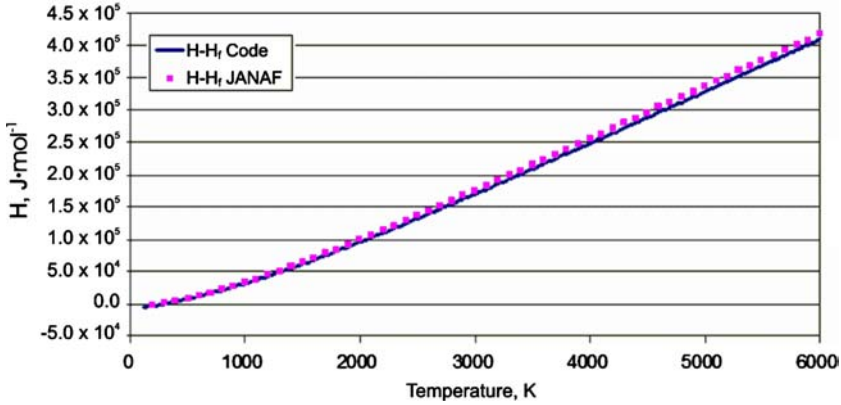

Fig. 6. Comparison of the enthalpy at constant pressure, H.

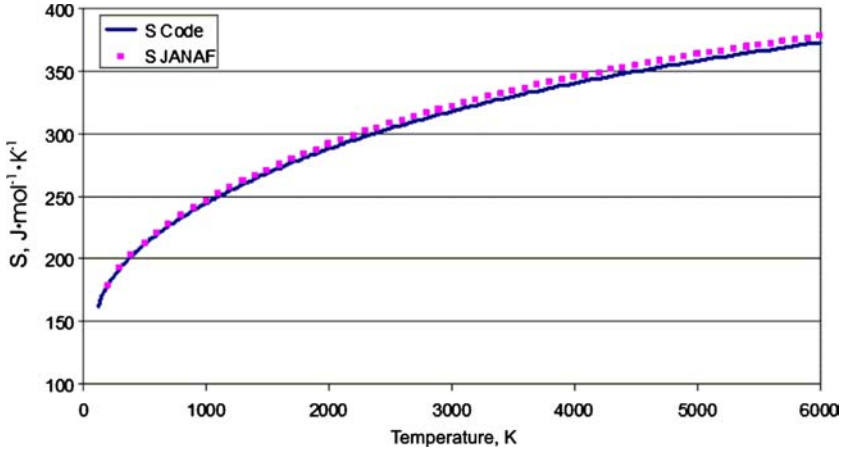

Fig. 7. Comparison of the entropy at constant pressure, S.

The discrepancy is trivial and expected as the JANAF data are several decades old and therefore the fundamental data used to calculate the thermochemical model have since been updated, e.g., vibrational mode frequency, and the calculation tool's accuracy has also increased. Quantitatively, the maximum percent variance for the specific heat, enthalpy, entropy, and Gibbs free energy comparisons are only 3.62%, 4.70%, 1.38%, and 1.18%, respectively.

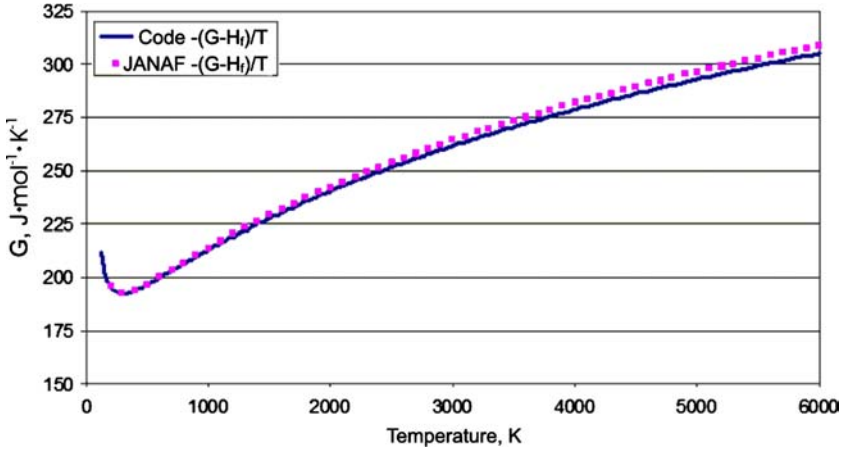

Fig. 8. Comparison of the Gibbs free energy at constant pressure, G.

4.2. Comparisons with Boulos et al.

Unlike the JANAF tables, the thermodynamic properties calculated by Boulos et al. [15] do include chemical reactions and also include a temperature range where ionization occurs. As mentioned above, ammonia is not included in any reactions; however, N_2 and H_2 are. The same modified code as was used in the composition verification is used for the thermodynamic property comparison to Boulos et al. [15]. The variables that will be compared are the density and the enthalpy [17]. As the ammonia species was verified using the JANAF tables, all the other species that are present in the ammonia mixture are verified in the temperature range of Boulos et al. In the N_2 case, the temperature range of Boulos et al. only extends high enough to include the first, second, and third N ions to any significant degree. The code system includes these ions and also the higher ions up to the fully-stripped N^{+7} ion. Verifying the validity of the three lower ions with Boulos also leads to the conclusion that the higher ions' thermodynamic properties can be considered valid. This is because the code subroutines that calculate the thermodynamic properties of the lower ions are the same for the ions not included in the temperature range of Boulos et al. Also, the data used to perform these calculations are all from the same source, Moore's tables [18].

Figures 9–12 compare the code output and the data from Boulos et al. and display excellent agreement. These confirm the insignificance of the discrepancies identified in the composition comparisons as well as support the assumption to exclude certain chemical reactions that would only

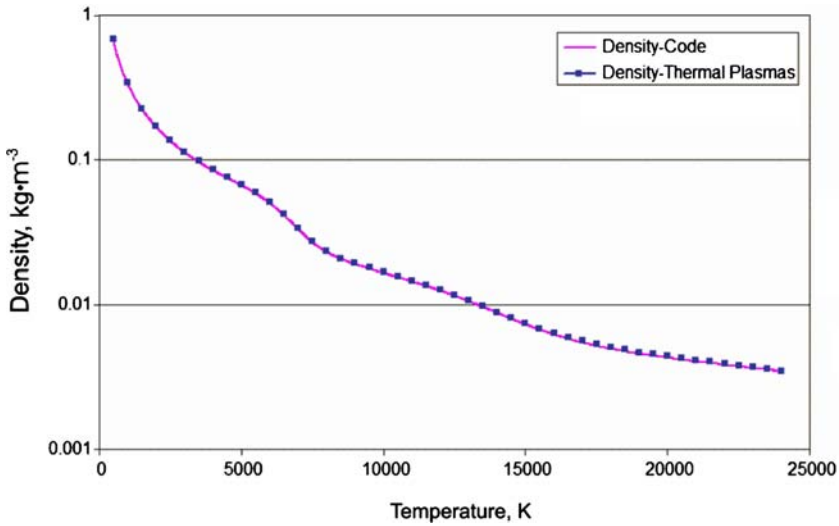

Fig. 9. Density code output compared to the density of Boulos et al. for nitrogen at 100 kPa.

increase computational time and perhaps error. There are other points that are noteworthy. The cut-off criterion used to find the correct limits on the sum of the electronic partition function were evidently the same or similar between Boulos et al. and the present code system, Eq. (16). Calculation of the thermodynamic properties in the higher temperature range can be extremely sensitive to the choice of the cut-off criterion. Also, the species that were neglected from the code system, but were included in the model of Boulos et al. do not affect the thermodynamic properties of the mixture. This indicates that the molecular and negative ions were indeed properly neglected from the code mixture.

5. EQUATION-OF-STATE RESULTS

5.1. Composition

The composition results are presented in two categories. The first addresses the lower temperature range where the neutral particles dominate, $0.00862\,\text{eV} < T_e < 1\,\text{eV}$ ($1\,\text{eV} = 11605\,\text{K}$), and the latter represents the higher temperature range where the ions and electrons are the prevailing species (up to $T_e = 50\,\text{eV}$). Representative results for different densities and temperature ratios, θ, are shown in Figs 13 to 18. These charts can be

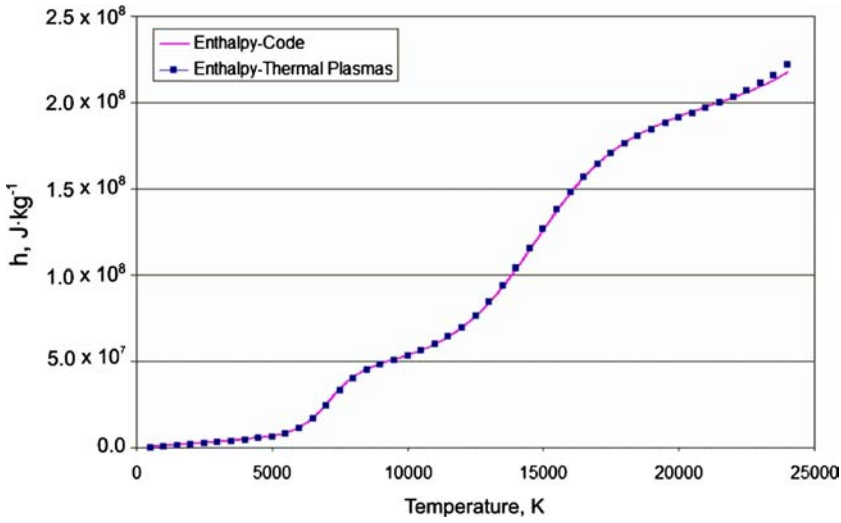

Fig. 10. Enthalpy code output compared to the enthalpy of Boulos et al. for nitrogen at 100 kPa.

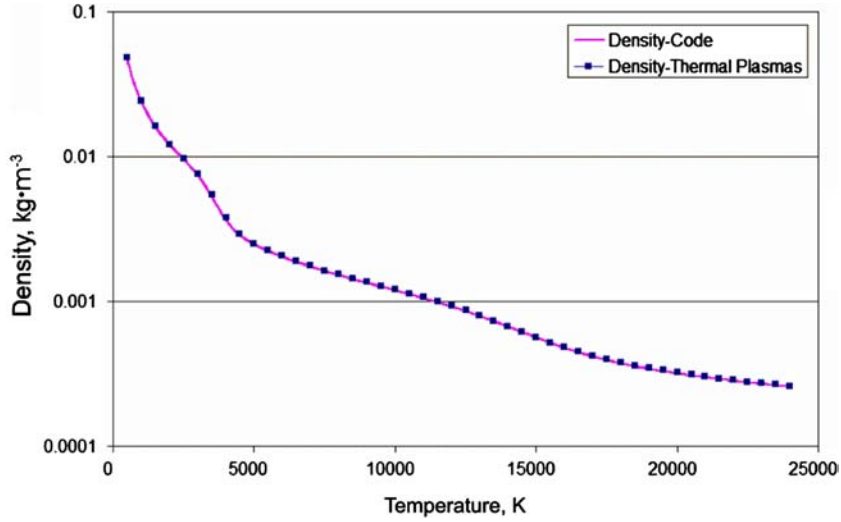

Fig. 11. Density code output compared to the density of Boulos et al. for hydrogen at 100 kPa.

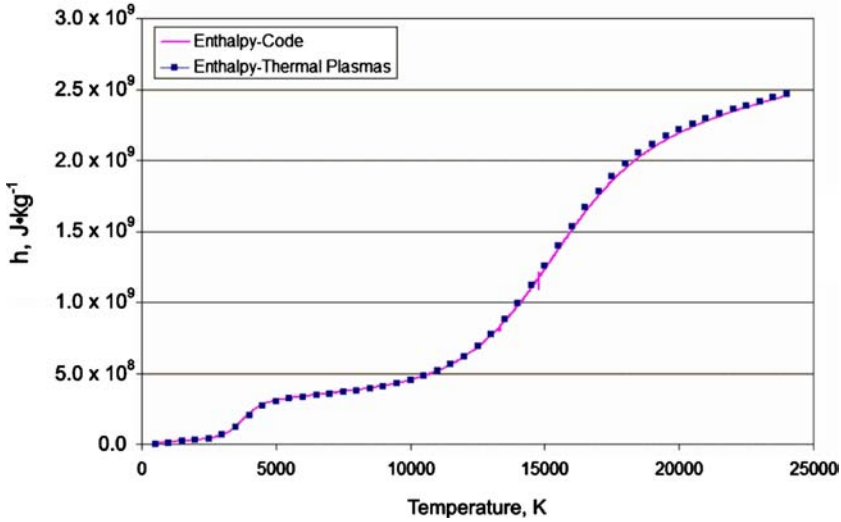

Fig. 12. Enthalpy code output compared to the enthalpy of Boulos et al. for hydrogen at 100 kPa.

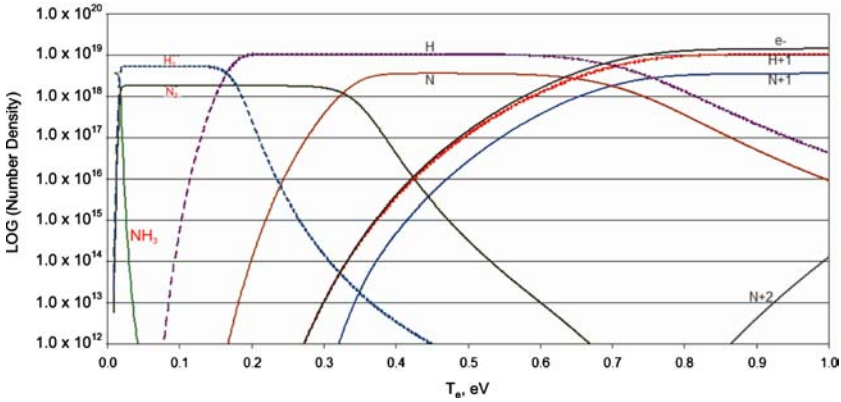

Fig. 13. Composition for $\theta = 1$ and $\rho = 1.0 \times 10^{-7}\,\mathrm{kg{\cdot}m^{-3}}$ and for the electron temperature range of $0.00862\,\mathrm{eV} < T_e < 1.0\,\mathrm{eV}$ ($1\,\mathrm{eV} = 11605\,\mathrm{K}$).

examined and general trends can be identified over the ρ, T_e, and T_h range of interest.

Noteworthy trends arise that serve as further confirmation of the model such as the decreasing ionization degree as the density increases at constant θ. Indeed, as expected, the electron temperature value at which higher nitrogen ions begin to dominate decreases with decreasing density.

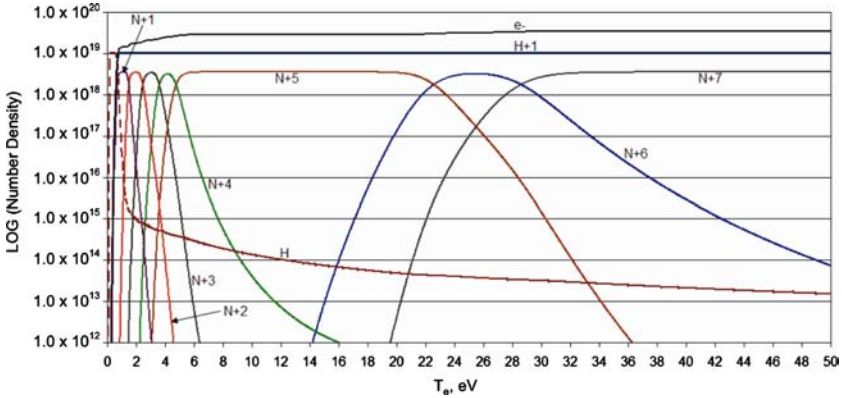

Fig. 14. Composition for $\theta = 1$ and $\rho = 1.0 \times 10^{-7}\,\mathrm{kg{\cdot}m^{-3}}$ and for the electron temperature range of $0.00862\,\mathrm{eV} < T_e < 50\,\mathrm{eV}$ ($1\,\mathrm{eV} = 11605\,\mathrm{K}$).

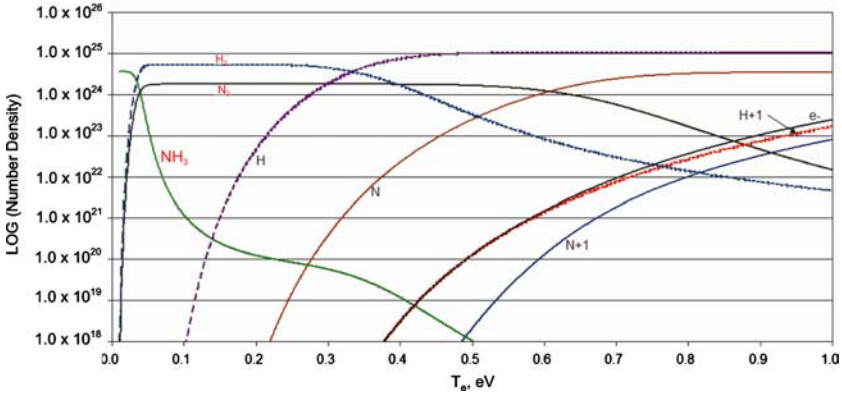

Fig. 15. Composition for $\theta = 1$ and $\rho = 1.0 \times 10^{-1}\,\mathrm{kg{\cdot}m^{-3}}$ and for the electron temperature range of $0.00862\,\mathrm{eV} < T_e < 1\,\mathrm{eV}$ ($1\,\mathrm{eV} = 11605\,\mathrm{K}$).

Furthermore, as θ is increased (by decreasing T_h) at constant density over the electron temperature range, there is almost no effect to the composition of higher ions. This is not surprising as the electron temperature is the principal factor in chemical reactions [19]. Therefore, as the heavy-particle temperature is decreased in relation to the electron temperature, the reactions that the mixture undergoes in the ionization temperature region are not noticeably altered.

However, when the T_e range of 0.00862 to 1.0 eV is examined, then it becomes clear that as θ is increased the neutral particles dominate at increasingly higher T_e values. The most likely explanation is because

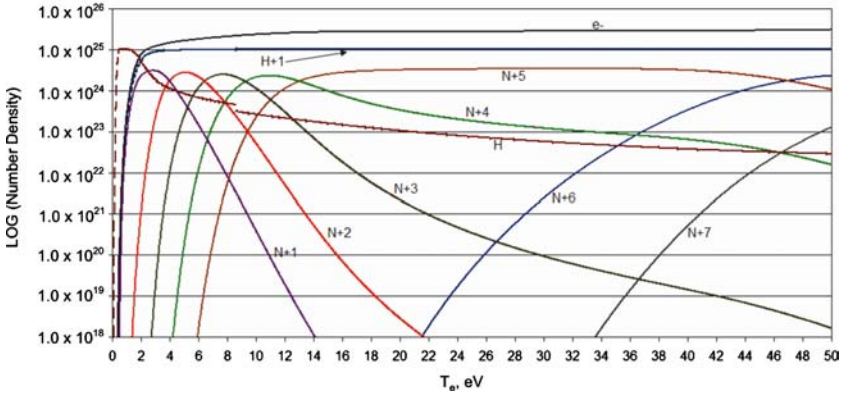

Fig. 16. Composition for $\theta = 1$ and $\rho = 1.0 \times 10^{-1}\,\mathrm{kg{\cdot}m^{-3}}$ and for the electron temperature range of $0.00862\,\mathrm{eV} < T_e < 50\,\mathrm{eV}$ ($1\,\mathrm{eV} = 11605\,\mathrm{K}$).

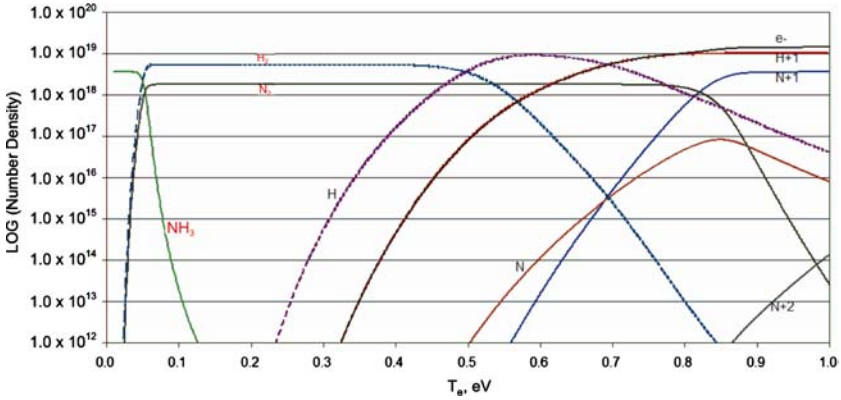

Fig. 17. Composition for $\theta = 3$ and $\rho = 1.0 \times 10^{-7}\,\mathrm{kg{\cdot}m^{-3}}$ and for the electron temperature range of $0.00862\,\mathrm{eV} < T_e < 1\,\mathrm{eV}$ ($1\,\mathrm{eV} = 11605\,\mathrm{K}$).

at higher θ values, the T_h value is correspondingly smaller. Due to the quasi-neutrality condition, there is a negligible amount of electrons present in the mixture when the neutral particles are dissociating only. Therefore, the mixture composition is almost independent of T_e variations. The only effect on the mixture would be due to the decreased heavy-particle temperature value, T_h. This extends the T_e temperature range that the neutral particles dominate. For example, at a constant density of $1.0 \times 10^{-5}\,\mathrm{kg{\cdot}m^{-3}}$, if $\theta = 1$ then NH_3 drops off the concentration scale at about $T_e = 0.075\,\mathrm{eV}$. But, for the same density and $\theta = 3$, NH_3 drops off the concentration scale at about $T_e = 0.21\,\mathrm{eV}$ ($0.075 \times 3 = 0.225$).

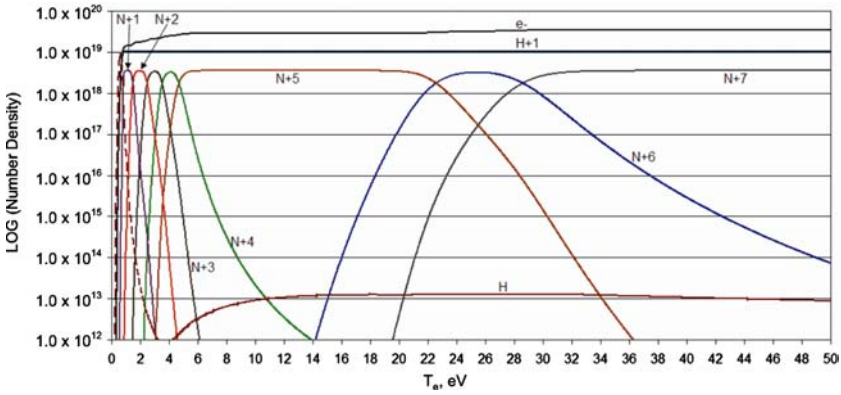

Fig. 18. Composition for $\theta = 3$ and $\rho = 1.0 \times 10^{-7}\,\mathrm{kg{\cdot}m^{-3}}$ and for the electron temperature range of $0.00862\,\mathrm{eV} < T_e < 50\,\mathrm{eV}$ ($1\,\mathrm{eV} = 11605\,\mathrm{K}$).

A further check on the composition results can be performed by examining at the ionization potentials of the atomic species and their ions as shown in Table I. As was observed in Figs. 14, 16, and 18, the N^{+5} ion is the dominant nitrogen species in the plasma mixture for a large electron temperature range. Table I illustrates why this is the case. The energy required to ionize an N^{+5} ion is over 22 times the energy required to ionize an N^{+4} ion. Thus, a much greater temperature (thermal energy) increase is required in order to reach a regime where the N^{+6} ion will be dominant. Other composition results can be confirmed using Table I as well. For example, the T_e range where N^{+6} is dominant is much larger than the first four ions and N^{+7} does not significantly appear in the mixture until very high T_e, etc.

5.2. Thermodynamic Properties

Similar to the composition results, some general trends can be identified from the thermodynamic properties that can further the insights into ammonia's thermochemistry throughout the ρ, T_e, and T_h range investigated with the current model. The two main thermodynamic properties addressed for this purpose are the specific internal energy (e) and the number of free electrons per heavy particle (*nfe*).

The number-of-free-electron-per-heavy-particle profiles vary more significantly as a function of density rather than as a function of θ. When the density is held constant and θ is changed from 1/2 to 3, there does not seem to be much change with *nfe*. This is not surprising as *nfe* is closely coupled with the composition as it is a measure of the average charge of

Table I. Ionization Potentials (IP) of Atoms and Their Ions Plus the Energy Difference Between Species' Ionization Potentials in eV ($1\,\text{eV} = 1.602 \times 10^{-19}$ J) [16].

Species	Ionization Potential [eV]	IP Difference Form Lower Ion [eV]
H	13.598	N/A
H+1	N/A	N/A
N	14.534	N/A
N+1	29.601	15.067
N+2	47.448	17.874
N+3	77.472	30.024
N+4	97.888	20.416
N+5	552.057	454.169
N+6	667.029	114.972
N+7	N/A	N/A

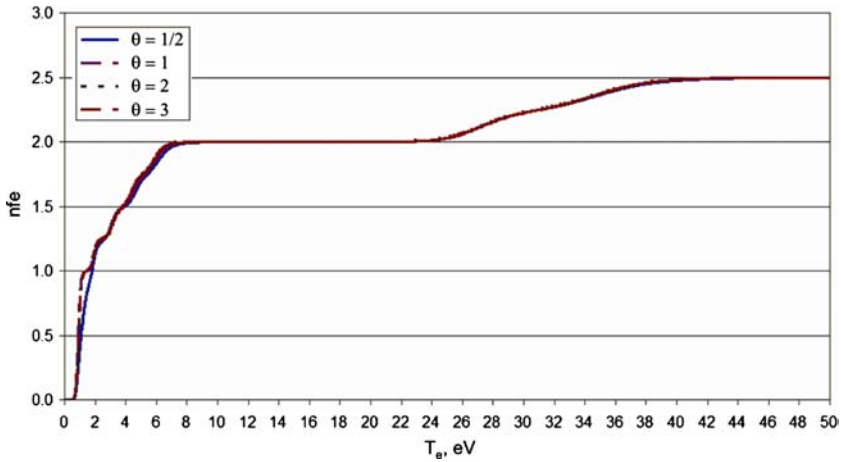

Fig. 19. Number of free electrons per heavy particle for varying temperature ratio at constant density ($\rho = 1.0 \times 10^{-5}\,\text{kg}\cdot\text{m}^{-3}$).

the mixture. For example, when the mixture is entirely made up of neutrals, then *nfe* is identically zero. From the last section, it was made clear that the composition in the ionization temperature range is subject to minimal changes for variable θ at constant density. This translates into almost no change in the *nfe* curves under the same conditions. Figure 19 shows an example of just such a case for $\rho = 1.0 \times 10^{-5}\,\text{kg}\cdot\text{m}^{-3}$.

When the density is varied at constant θ, the distinction of the ionization process becomes more apparent. Several progressive plateaus are identified as the mixture proceeds to sequentially ionize. The most distinctive

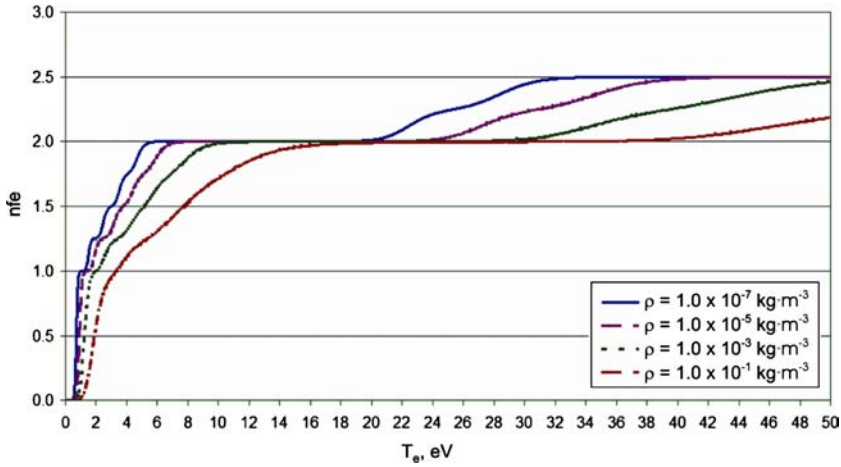

Fig. 20. Number of free electrons per heavy particle for varying density at constant temperature ratio ($\theta = 2$).

plateau, as shown in Fig. 20 at a value of $nfe = 2.0$, represents domination of the N^{+5} ion as the subsequent N ions' formation is delayed due to their substantially higher ionization potentials. It is also noteworthy and expected that the substantial ionization ensues at lower electron temperature values as the mixture's density (or pressure) is decreased.

The specific internal energy follows a fairly predictable curve in all cases. Generally, as the mixture stays at a fairly constant composition over some T_e range, the specific internal energy variation will be linear. However, over the T_e range where reactions occur, such variation is expected to display a steeper positive slope that represents energy deposition to the internal modes of the gas as opposed to heating as shown in Figs 21 and 22.

The same expected trends are evident as the specific internal energy is inspected as a function of density at constant θ. In this particular case, however, the successive ionization processes are more exaggerated by the evident distinctive steeper positive slopes which of course represent deposition to internal energy modes at approximately constant temperature. The most profound is nitrogen's fifth-level ionization, N^{+5}, which occurs at increasing T_e values with increasing density. It is noteworthy, that for a substantial range of electron temperature, the mixture consists of only singly-ionized hydrogen and these N^{+5} ions, ($5\,\text{eV} < T_e < 20\,\text{eV}$) without varying substantially with density. This can be useful for applications that would tend to operate within such a regime and thus could allow approximation of the caloric equation of state as simply $\Delta e = C_v \Delta T$, where C_v is the specific heat at constant volume. In addition, the expected independence of such slope (C_v), on density is clearly evident in Fig. 22.

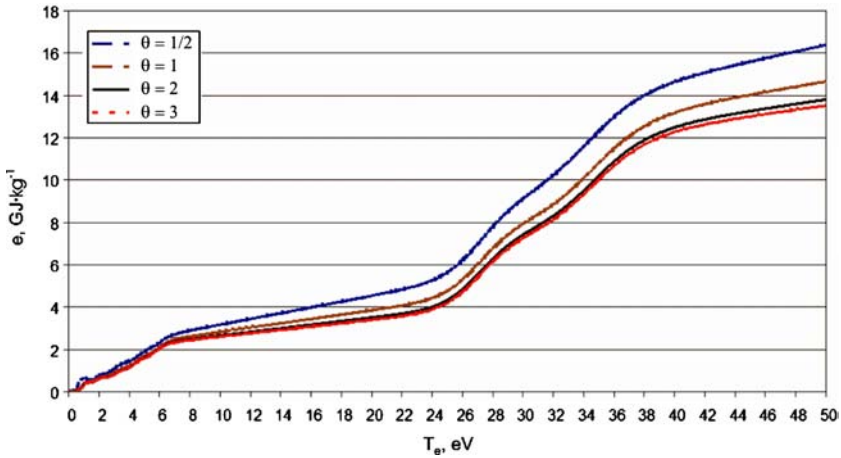

Fig. 21. Specific internal energy for varying temperature ratio at constant density ($\rho = 1.0 \times 10^{-5}\,\mathrm{kg{\cdot}m^{-3}}$).

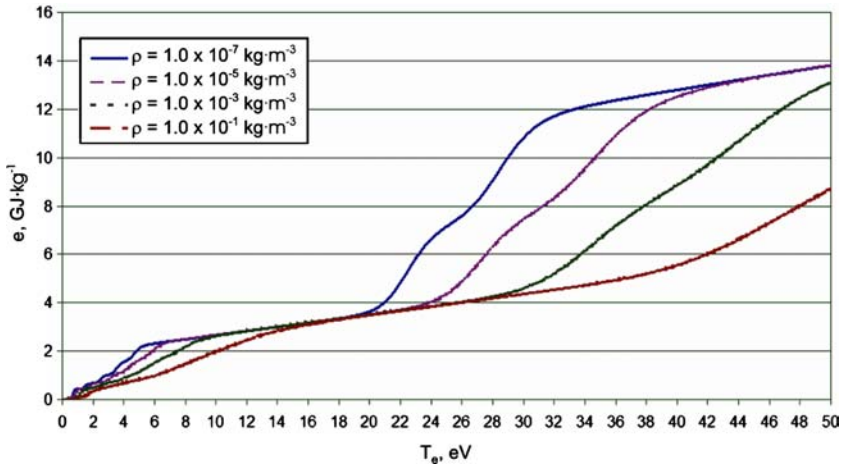

Fig. 22. Specific internal energy for varying density at constant temperature ratio ($\theta = 2$).

In this and the N^{+7} dominated temperature intervals, a simplified equation for the internal energy can be used as a further check of the code output. This caloric equation of state is represented by

$$\Delta e = C_v \Delta T = (\overline{\varsigma} + 1)\left[\frac{R}{\overline{M}\,(\gamma - 1)}\right]\Delta T \tag{26}$$

where $\overline{\varsigma}$ is the average charge or nfe, R is the universal gas constant, $\overline{M}$ is the average atomic mass of the mixture and γ is the ratio of specific

heats. The slope, or C_v, can be calculated where *nfe* is constant and the mixture is known. Over the range where the mixture is almost entirely made up of only the e^-, H^+, and N^{+5} species, the code calculated a C_v value of 8787.8 $GJ \cdot kg^{-1} \cdot K^{-1}$ whereas using Eq. (26) a value of 8787.8 $GJ \cdot kg^{-1} \cdot K^{-1}$ is also calculated. When the mixture is effectively made up of only the e^-, H^+, and N^{+7} species, the code calculated a C_v value of 10252.4 $GJ \cdot kg^{-1} \cdot K^{-1}$ and Eq. (26) calculates a value of 10252.4 $GJ \cdot kg^{-1} \cdot K^{-1}$ as well. Such a comparison serves as further verification as no models were available at this very high temperature range.

6. CONCLUSIONS

An ammonia thermal non-equilibrium equation of state has been developed for density and temperature values encompassing $1.0 \times 10^{-7}\,kg \cdot m^{-3} < \rho < 1.0 \times 10^{-1}\,kg \cdot m^{-3}$ and $0.00862\,eV < T_e < 50\,eV$ and a varying temperature ratio, $\theta = T_e/T_h$. The output can be easily cast in convenient tabular form to complete the set of the familiar conservation equations used by hydrodynamic and/or magnetohydrodynamic computer codes.

The chemically-reacting mixture's composition and thermodynamic properties are computed under ideal-gas and local thermodynamic equilibrium assumptions and have been verified by comparisons to similar, but limited models. Specifically, Beaumont's model included the dissociation temperature ranges while JANAF's temperature range was from 100 to 6000 K. Boulos et al. had the most extensive temperature range that included dissociation and ionization, 100 to 25000 K, although it did not include the ammonia species but only nitrogen and hydrogen. In addition, all the aforementioned models were calculated under a one-temperature assumption.

Inspection of the ammonia properties' behavior identifies general trends for the composition and thermodynamic properties over the range of ρ, T_e, and T_h considered in this effort. All behaviors are explained with physical arguments and are displayed in Figs 19 to 22. Specifically, the electron temperature range within which species will dominate the composition become progressively greater as the density is increased. Also, the electron temperatures at which neutrals will dominate the composition become progressively greater as the temperature ratio (θ) is increased. Otherwise, the composition is slightly affected at constant density but veriable Q.

General trends for the thermodynamic properties of the number of free electrons (*nfe*) and the specific internal energy (e) were also observed. The *nfe* property followed the composition observations closely. That is, the density is the main factor in deviations from one curve to the next,

while θ had little effect. Likewise, for e, the density had the greatest impact. However, as shown in Eq. (27) shown below for convenience,

$$e = R_i T_i^2 \left(\frac{\partial \ln Q^{\text{tot}}}{\partial T} \right)_{N,V} \tag{27}$$

the specific internal energy does rely on a parabolic relationship with temperature. Therefore, as θ is increased, there is increasingly little difference between the different e profiles over the T_e range when electrons are the dominant species (almost and fully ionized mixtures). However, at low θ (high T_h), there is greater disparity between curves at constant density.

ACKNOWLEDGMENT

This work was partially funded by the NASA Glenn Research Center.

REFERENCES

1. W. D. Deininger, A. Chopra, T. J. Pivirotto, K. D. Goodfellow, and J. W. Barnett, *The 30-kW Ammonia Arcjet Technology Final Report* (NASA-CR-186850, JPL Publication 90–4, Feb. 15, 1990).
2. C. Lee Dailey and Ralph H. Loveberg, *The PIT MkV Pulsed Inductive Thruster* (NASA Contractor Report 191155, NASA Lewis Research Center, Cleveland, 1993).
3. B. Beaumont, P. Gibart, and J. P. Faurie, *J. Crystal Growth* **156**:140 (1995).
4. M. I. Boulos, P. Fauchais, and E. Pfender,*Thermal Plasmas* (Plenum Press, New York, 1994), pp. 255, 258, 259.
5. C. J. Cramer, *Essentials of Computational Chemistry: Theories and Models*, 2nd Ed. (John Wiley & Sons, Chichester, 2004), pp. 359–365.
6. J. D. Anderson, Jr., *Hypersonic and High-Temperature Gas Dynamics* (American Institute of Aeronautics and Astronautics, Reston, 2000), pp. 437–438.
7. A. B. Cambel, D. P. Duclos, and T. P. Anderson, *Real Gases* (Academic Press, New York, 1963), p. 42.
8. M. Venugopalan, *Reactions Under Plasma Conditions* (John Wiley & Sons, New York, 1971), Vol. 1, pp. 65, 66.
9. L. Couture and R. Zitoun, *Statistical Thermodynamics and Properties of Matter* (Gordon and Breach Science Pubs., Australia, 2000), pp. 125, 126.
10. C. J. Cramer, *Essentials of Computational Chemistry: Theories and Models* (John Wiley & Sons Ltd., Chichester, 2004), p. 358.
11. A. B. Koudriavtsev, R. F. Jameson, and W. Linert, *The Law of Mass Action* (Springer, Berlin, 2001), p. 57.
12. J. D. Anderson, Jr., *Hypersonic and High Temperature Gas Dynamics* (American Institute of Aeronautics and Astronautics, Reston, 2000), p. 457.
13. J. D. Anderson, Jr., *Hypersonic and High Temperature Gas Dynamics* (American Institute for Aeronautics and Astronautics, Reston, 2000), pp. 453–457.
14. C. J. Cramer, *Essentials of Computational Chemistry: Theories and Models* (John Wiley & Sons Ltd., Chichester, 2004), pp. 366–370.

15. M. I. Boulos, P. Fauchais, and E. Pfender, *Thermal Plasmas* (Plenum Press, New York, 1994), Vol. 1, pp. 237–238.
16. M. W. Chase, Jr., *J. Phys. Chem. Ref. Data: NIST-JANAF Thermochemical Tables,* 4th Ed., Monograph No. 9, Parts 1 & 2 (American Institute of Physics and the American Chemical Society, Woodbury, New York, 1998).
17. M. I. Boulos, P. Fauchais, and E. Pfender, *Thermal Plasmas* (Plenum Press, New York, 1994), Vol. 1, pp. 389–407.
18. C. E. Moore, in *Tables of Spectra of Hydrogen, Carbon, Nitrogen, and Oxygen Atoms and Ions*, Jean W. Gallagher, ed. (CRC Press, Boca Raton, 1993).
19. R. W. Humble, G. N. Henry, and W. J. Larson, *Space Propulsion Analysis and Design, Revised*, 1st Ed. (McGraw-Hill, New York, 1995), p. 546.